INL/CON-21-65110-Revision-0

Modeling of ATR Fuel in DOE Standard Canisters with Helium Backfill

March 2022

Alexander W Abboud

Changing the World's Energy Future

Idaho National Laboratory

INL/CON-21-65110-Revision-0

Modeling of ATR Fuel in DOE Standard Canisters with Helium Backfill

Alexander W Abboud

March 2022

Idaho National Laboratory
Idaho Falls, Idaho 83415

http://www.inl.gov

Prepared for the
U.S. Department of Energy
Under DOE Idaho Operations Office
Contract DE-AC07-05ID14517

Modeling of Spent ATR Fuel in DOE Standard Canisters with Helium Backfill – 22316

Alexander W. Abboud*
* Idaho National Laboratory, 1955 Freemont Ave., Idaho Falls, ID 83415

ABSTRACT

One pathway for road-ready and final disposition packaging configurations for the aluminum-clad spent nuclear fuel (ANSF) fuel is storage within helium backfilled sealed Department of Energy (DOE) standard canisters. The typical packaging configuration for the 15-foot DOE standard canisters places 10 advance test reactor (ATR) elements a basket, and three baskets are loaded within each DOE canister. During in-reactor operations and cooling pond storage conditions, oxyhydroxide layers form on the surface of the aluminum clad fuel. These layers produce hydrogen gas over time due to the fuel's radiation field. As part of the packing procedure, the ATR fuel should be dried to remove any residual physio-/chemi- sorbed water bound to the surface.

A 50-year CFD model of the DOE canister packaged with fuel was developed to provide a temperature profile for coupled chemical modeling of the conditions within the canister. The results of this modeling include results at fully saturated and fully dried fuel cladding conditions. In the associated experimental work, radiolysis experiments tests were completed in a helium environment, and G-values for the radiolytic production of hydrogen from the oxyhydroxide layers were provided. That reaction was coupled with the thermal profiles and gas-phase reactions to develop a 50-year model of the conditions within a sealed DOE canister with ATR fuel. For a nominal scenario of stored ATR fuel, after 50 years the model results give a 1.36 atm total pressure, 7% mole percent hydrogen, for the upper decay heat, 1.51 atm total pressure, 16% mole percent hydrogen, and for upper decay heat with undried fuel 2.6 atm total pressure, 15% mole percent hydrogen. No case modeled yields significant oxygen, and for the lower decay heat case that is modeled, hydrogen concentrations are under the 4% flammability limit after 50 years of storage. The modeled pressures for all cases modeled are below the pressure limit for the DOE standard sealed canister.

INTRODUCTION

By the year 2035, there will be ~2500 MTHM of spent nuclear fuel (SNF) that will require geologic repository disposal that is managed by DOE. Approximately 400 MHTM of this is currently not packaged. Previous studies in support of geologic disposal divided the DOE SNF inventory into 34 groups based on fuel matrix, cladding, cladding condition and enrichment [1]. The six aluminum clad fuel types are of interest as aluminum is significantly less corrosion resistant than stainless steel and zircaloy clad fuel. The aluminum cladding develops a corrosion layer that generates hydrogen from radiolysis, and that contain bound, both physiosorbed and chemisorbed, water. While there is a wide range of enrichment and burnup profiles across the DOE spent fuel inventory, the focus herein is on the spent ATR fuel stored at INL.

One disposition path for the fuel is packaging and shipping in DOE standard canisters which are "road-ready" storage when dried and backfilled with helium. The fuel is removed from wet storage, dried to remove residual water then placed in packing configurations inside DOE standard canisters which are backfilled with helium and sealed. A previous study examined the chemical contents within the DOE canisters using a set of radiolytic chemistry reactions for both the gas and the aluminum surface. The previous report utilized G-values for the surface reactions in an argon atmosphere, but recent experimental tests have calculated corrected values for a helium environment [2]. These tests also show deviation from linearity with increasing dose, indicating a potential steady-state H2 concentration, though higher dose samples are to be evaluated in the future.

The modeling here solves for the thermal fields using a computational fluid dynamics (CFD) model of the ATR spent fuel storage configuration, which should bound most scenarios for intact fuel of the DOE ASNF inventory. The assumption in this model is that all the fuel is intact, and no breach of cladding has occurred. The flow in storage containers of spent nuclear fuel is primary driven through natural convection as air is heated from the central fuel and cooled by the outer air, shown both experimentally and in numerical computational fluid dynamics (CFD) simulations [3,4,5,6,7,8,9,10]. Improvements to basic models have used commercial packages to fully resolve the fuel configurations in lieu of coarse-resolution porous media models [6]. Many of these CFD models have not coupled the thermal and convective fields with the harmful chemical species which occur due to the radiolytic breakdown of water vapor, nitrogen, oxygen and carbon dioxide that can be within canisters [11,12,13]. The developed transient model that is used here allows for one-way coupling of the transient thermal environment of the DOE sealed canisters with the full set of radiolytic chemical reactions for both gas phase and surface phase chemistry [14]. This study uses prior CFD-thermal simulations of the DOE standard canisters which were coupled with the gaseous radiolytic reactions and aluminum oxyhydroxide radiolytic reactions. This model utilizes the full set of 115 gas phase reactions, coupled with the aluminum oxyhydroxide surface reactions. The G-values here have been updated from the previous DOE canister reports [15] and model updates have been made to apply the G-values to the total aluminum mass.

The thermal field of gas, spent ATR fuel, and other components stored in sealed standard DOE canisters, as well as the dose rates for the fuel cladding surface were resolved over a 50-year period. This data was coupled with a Cantera model to solve for the full radiolytic chemistry associated with sealed DOE canisters of these ASNF with G-values for hydrogen from the corrosion surface in a helium environment.

METHODS

A summary of previously constructed model is provided. More in depth details are provided in other reports [14,15]. There are three main changes to the initial model that were made here. The first is that the radiolytic yield of hydrogen from the oxyhydroxide layers has been updated to be dependent on the dose delivered to the entire sample weight, rather than the oxyhydroxide layer weight, which was determined to be more consistent with ongoing experiments. The second change is the G-value has been updated from the argon environment experiments to helium environments, causing a decrease of more than 50% to the G-value. The third is that both undried and dried conditions of the aluminum oxyhydroxide film on the ASNF fuel are also included here.

Thermal-Fluid Model

The commercial multiphysics modeling platform STAR-CCM+ is used for modeling the canister [16]. The numerical solver implemented here is a finite-volume approach with second-order implicit time stepping and a second-order discretization scheme. The segregated flow solver for the Navier-Stokes equations is used, which is applicable to constant density or mildly compressible flows, with a predictor-corrector approach that couples the momentum and continuity equations. A collocated variable arrangement with a Rhie-Chow scheme for pressure-velocity coupling is implemented in a SIMPLE-type algorithm [16]. In the canister scale models, the Reynolds is low enough such that laminar flow is assumed. The momentum equation is then given by

(Eq. 1)

Where is the velocity vector, , is the stress tensor, and is the density. The term is the body force, solely occurring due to the buoyancy driven flow in this case. The viscous stress tensor is

(Eq. 2)

Where is the air viscosity. The mass conservation is expressed through the continuity equation

(Eq. 3)

The conservation of energy gives an equation in terms of the total energy, , as

(Eq. 4)

Where in the solid phases, the terms with are equal to 0, is the conductive heat flux, the energy source term is due to the chemical reactions in the fluid phase, and is from the specified heat source for the fuel plates in that solid region. The implicit solver in Star-CCM+ can typically adapt up to a Courant-Friedrichs-Lewy (CFL) condition of nearly 50. The properties for the materials used for each of the solid regions are shown in TABLE I, it is assumed maximum temperatures are low enough to use constant thermal properties for solids. The temperatures used utilize a 5-environment histogram of temperatures to account for the thermal gradient in the canisters.

TABLE I. Physical properties of the components for a DOE Standard Sealed canister.

Material	**Density [kg/m^3]**	**Thermal Conductivity [W/m K]**	**Heat Capacity [J/kg K]**	**Emissivity [-]**
Al-6061 (siding/back plates) [17]	2702	167	896	0.82
Stainless Steel 304 [18]	7900	14.9	477	0.46
Stainless Steel 316 [18]	8238	13.4	468	0.46
Carbon Steel [18]	7854	60.5	434	0.89
ATR Fuel Plates [19]	3680	42.6	614	0.82 (assumed)

Model Geometry

For a DOE standard canister loaded with ATR spent fuel, the loading configuration is described in Kim et. al., with the basket configuration described in DOE/SNF/REP-90 and minor modifications for tolerance included in DOE/REP/DSN-19 [20,21,22]. The loaded configuration uses the 4.57 m long, 0.457 m inch diameter (15 feet long, 1.5 feet diameter), configuration of the DOE standard canister constructed of stainless steel 316. Inside this are 3 Type 1a baskets, previously assumed to be made of stainless steel 304.

The fully loaded canister configuration used in the previous CFD model is shown in Fig. 1a, with the ATR fuel CAD shown in Fig. 1b, and the Type 1a basket is shown in Fig. 1c. Fig. 1d shows a horizontal slice of the meshed domain used in the CFD simulations. The red denotes the fuel plates, the blue denotes

the free volume of air, the light grey shows the aluminum side plates, the medium grey shows the basket, and the outer dark grey shows the canister.

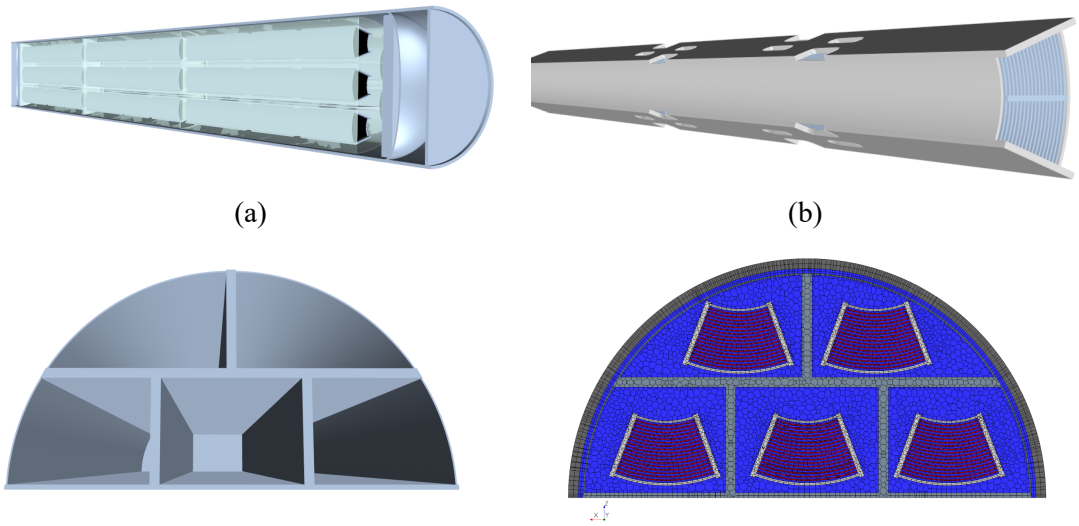

(a) (b)

(c) (d)

Fig. 1. Half domain used in simulations showing (a) fully loaded canister, (b) a single ATR element, (c) a single Type-1a basket, and (d) a central horizontal mesh slice.

Thermal Decay Heat and Ambient Conditions

As with the prior reports, an assumption is made that yearly temperatures for a 50-year storage scenario would mimic the conditions seen in the Irradiated Fuel Storage Facility [14]. Ambient temperatures for the INL INTEC CPP-603 facility are described in Christensen [23,24]. A plot of the ambient temperature conditions measured when the facility had working thermocouples in 2011 is shown in Fig. 2a, with 9 thermocouples recording once an hour over a year long period. The data in Fig. 2b shows weeklong averages. The ambient temperature within the facility itself has a very small variation within it compared to the exterior climate due to the large amount of mass of spent fuel stored within it. The largest temperature difference in a 12-hour span is only 1.5° C, and largest temperature difference in a week-long span is 4.4° C. This justifies the large timesteps used for the CFD model for the thermal history. TABLE II includes the parameter ranges used in the study for residual water, oxide thickness and dried/undried cases. The H2O(g) is residual water that is left as water vapor due to the lack of condensation for the model, the 10% upper limit is the equivalent of 100% relative humidity at 50 C, which is only considered for the undried fuel scenario. The oxide thickness under a conservative assumption could be as high as 34 µm [25], though more recent analysis shows a range of 5-15 µm as more likely bounding values [26,27].

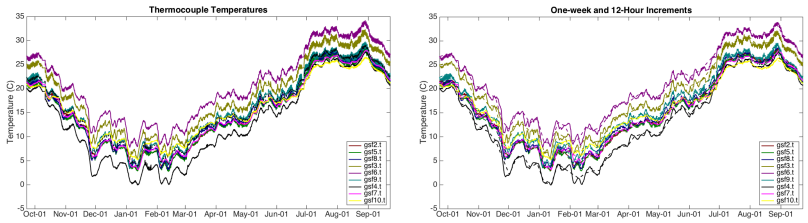

(a) (b)

Fig. 2. Thermocouple measurements over 1 year in the INL CPP-603 facility for (a) one-hour intervals, (b) 12-hour and weekly intervals.

TABLE II. Sensitivity parameters for this study.

Parameter	**Lower Bound**	**Base Case**	**Upper Bound**
Residual H_2O(g) [mol %]	0.1	1	10
Chemi-/Physio- sorbed water on ATR		1.01:1 H_2O to Al_2O_3	2.5:1 H_2O to Al_2O_3
Corrosion Layer Thickness [μm]	5	10	15
Decay Heat [W]	6	18	42

In ECAR 2906, MicroShield 9.01 was used to calculate the on-contact and 1-meter dosage rates for ATR fuel assemblies [28]. Based on the decay heat for a given fuel assembly, the on-contact dosage rate can be estimated as

(Eq. 5)

in units of Gy/s, with Q as the decay heat rate given in Watts by

(Eq. 6)

Chemical Equations Summary

As this model uses one-way coupling between the CFD simulation and the Cantera chemical solver, the full set of 115 gas phase reactions with 40 species from Wittman and Hanson 2015 is utilized here [29]. In the Wittman and Hanson study, the set of chemical reactions was built from three primary sources [11,12,13]. The appendix to Abboud and Huang 2019 contains the full set of chemical reactions implemented formatted for import into the Cantera code for solving the differential equations for the chemical system [30]. These gas phase reactions are then coupled with solid phase chemistry for the aluminum oxyhydroxide phase. A previous report showed the agreement of the aluminum oxyhydroxide surface chemistry modeling with regards to experimental data with small coupons [14]. The surface chemistry of the aluminum oxyhydroxide layer of the fuel was broken down into the radiolytic generation of hydrogen, given by

With the hydrogen radical determined through a combination of model tuning, and atomistic theory [31]. The G-value used here was updated from the previous work to be specific to a helium back-filled environment. For relative humidity of 100%, the G-value is 4.12×10^{-4} μmol/J, and for relative humidity of 50%, the G-value is 2.92×10^{-4} μmol/J, applied to the entire sample mass. This is a change from previous modeling efforts, which applied the G-value only to the mass of oxyhydroxide layer using the G-values [2]. This effectively changes the reaction from 1st order with regards to the corrosion layer to 0th order. Another reaction is included with a slow rate to convert the intermediate AlOO to stable Al_2O_3. The thermal dehydration of boehmite at low temperatures was also considered. The mass loss of aluminum oxyhydroxide coupons was considered to be from the loss of water in determining the kinetic rate according to the reaction

This reaction was fit to the mass loss of the coupons ranging from 25 to 180 °C [32]. For a conservative approximation on undried cases, the upper end of pseudo boehmite was assumed with a 2.5:1 H_2O to Al_2O_3 ratio [33]. Lastly, the general corrosion of aluminum if the oxyhydroxide layer was consumed was

also considered from an older study [34]. This reaction was adapted from aluminum in water rather than humid air, and so should be conservative to include

Though it should be noted this is the most minimal effect. At an average surface temperature of 50 °C, the total aluminum corrosion would only equation to 1.2 grams after 50 years, or 58 grams after 50 years at 200 °C surface temperature.

RESULTS AND DISCUSSION

Temperature and Velocity Fields

The CFD modeling for the temperature fields was completed for a steady state case for initialization of each of the three decay heats, and this was run for a transient time period to obtain a 50-year thermal profile. A set of horizontal slices for the initialized temperature for each of the fuel decay heats is shown in Fig. 3, with a-c for the low decay heat case, 3d-f for the nominal case, and 3g-i for the high decay heat case. Here the central basket shows hotter temperatures than the lower and upper, and the central fuel is the location for the highest temperatures. These temperature fields are used to create temperature bins in the Cantera chemical model to account for the temperature gradients. The corresponding velocity field are shown in Fig. 4a-c for the low decay heat case, in 4d-f for the nominal case and 4g-i for the high decay heat case. The 50-year canister average temperature is shown in Fig. 5 for all four of the storage configurations for the lower, nominal, and upper decay heat cases.

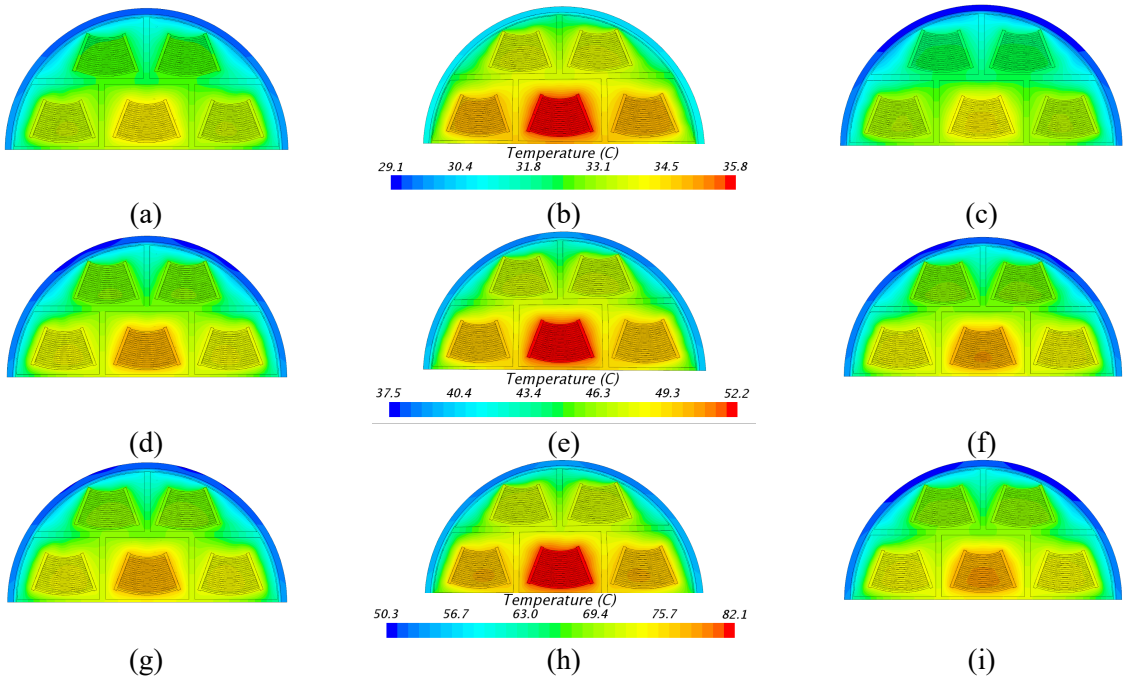

Fig. 3. The temperature for the low-decay heat case: (a) lower, (b) central and (c) upper horizontal plane; nominal case: (d) lower, (e) central and (f) upper horizontal plane and high-decay heat case: (g) lower, (h) central, and (i) upper horizontal plane.

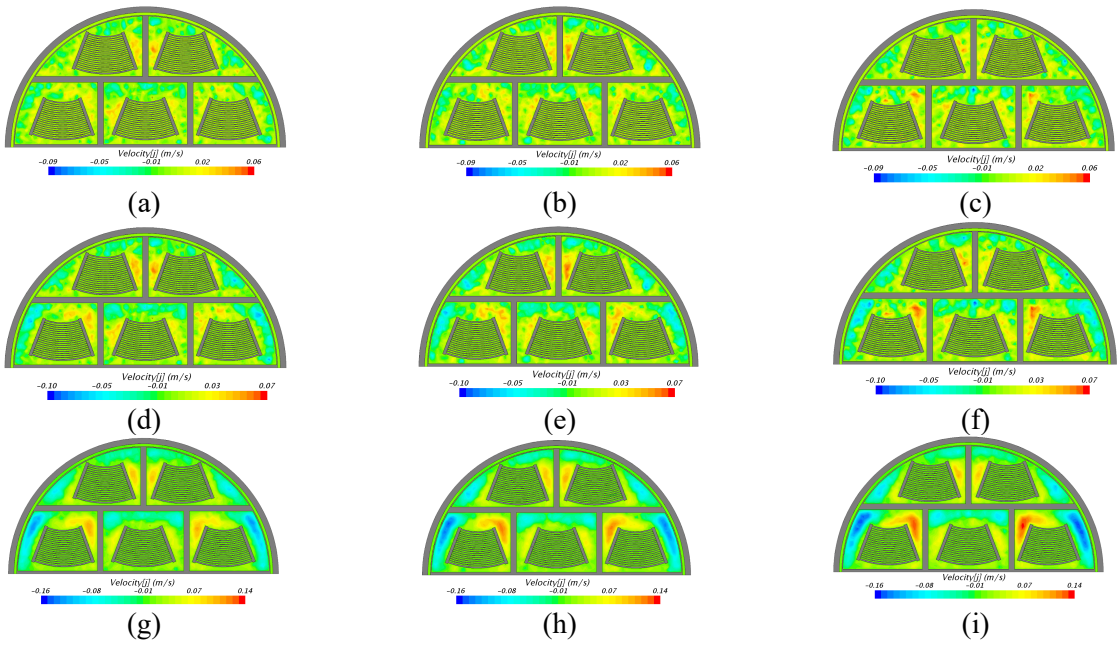

Fig. 4. Horizontal slice of the vertical velocity for low decay heat case at (a) lower (b) central and (c) upper baskets, for the nominal case in the (d) lower (e) central and (f) upper baskets, and for the high decay heat case for the (g) lower (h) central and (f) upper baskets.

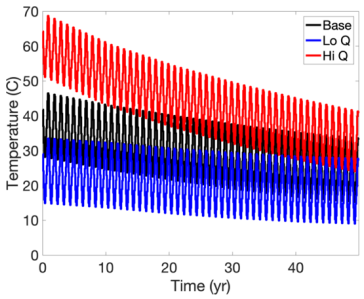

Fig. 5. The canister average temperature for spent ATR fuel over a 50-year time frame

Fully Dried Spent Fuel

The results in this section reflect a minimal bound water content of 1.01:1 H_2O:Al_2O_3 in the oxyhydroxide Fig. 6a shows the nominal case for the pressure increase over time, with a small increase at the very start of the model, growing to 1.36 atm total pressure after a 50-year period. Fig. 6b shows the nominal case for the different major species present. This confirms that with the changes to the model, combined with higher G-values, no shift in the possible corrosive species present is expected, so only hydrogen is present in significant quantities. Fig. 7a shows the cases for the differing decay heats and corrosion thicknesses for the pressure evolution over time, and Fig. 7b shows the hydrogen generation over that time period. The sensitivity to the decay heat shifts the pressure by about 0.25 atm and hydrogen content by 13 mole percent, while the sensitivity to the corrosion layer thickness is nearly negligible with variations of 0.03 atm and 0.1 mole percent. Of note, with the updated G-values the lower estimation of the fuel decay heat hydrogen value is less than the 4% flammability limit.

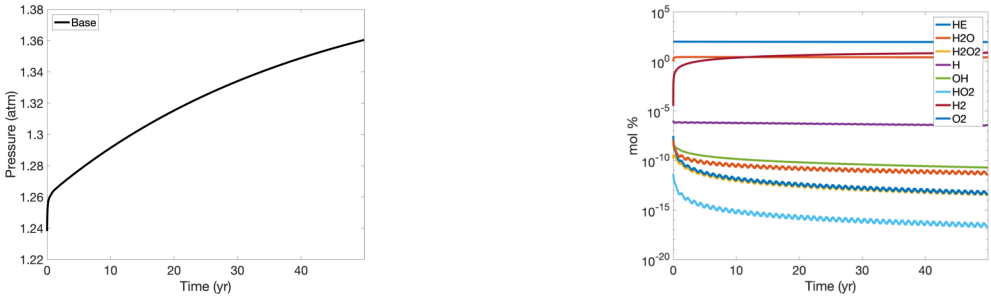

(a) (b)

Fig. 6. The (a) pressure increase for the nominal case, and (b) the speciation of the major chemical components present for the ATR fuel storage.

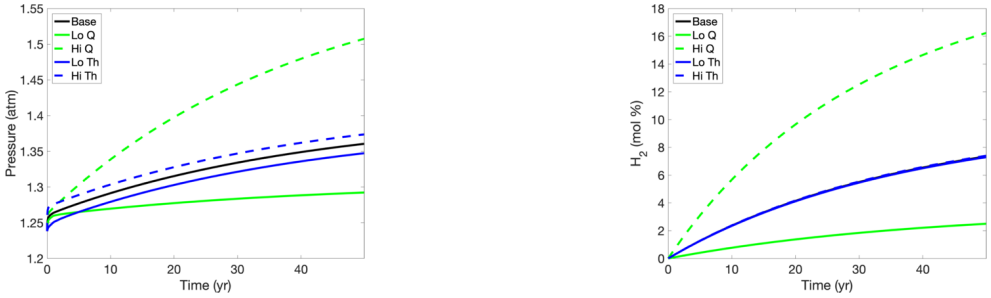

(a) (b)

Fig. 7. The (a) pressure increase for all cases, and (b) the hydrogen generated for all cases (Q = decay heat, Th = corrosion layer thickness) for ATR fuel storage.

For the case considered with 1% residual air present, the generation of hydrogen and the corresponding pressure are nearly identical. Fig. 8a shows the pressure increase for the nominal case, and Fig. 8b shows the major species for the nominal case. These again show that changes made to the model do not cause formation of other major species of concern present in large quantities other than hydrogen and nitric acid. Plots showing the decay heat and corrosion layer thickness differences are shown in Fig. 9a for the canister pressure, in Fig. 9b for the hydrogen content, and in Fig. 9c for the nitric acid content. None of the cases considered appear to have reached equilibrium with regards to nitric acid or hydrogen by the end of the 50-year model. The summary of the outcomes for the dried fuel cases both with and without the 1% residual air are shown in TABLE III. The differences with regards to nitric acid show a variation of about 2400 ppm as a function of decay heat and 30 ppm as a function of corrosion layer thickness.

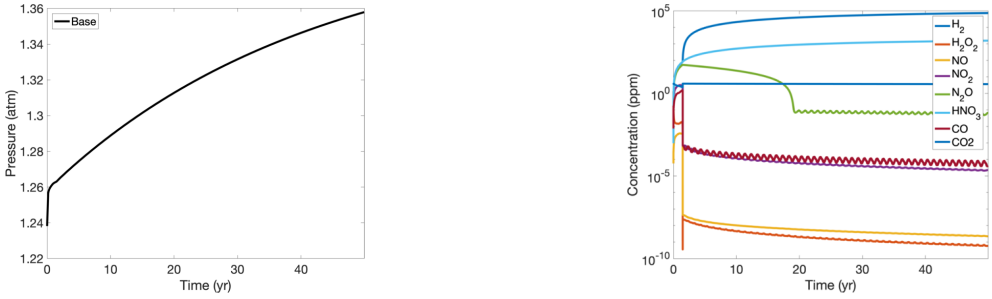

(a) (b)

Fig. 8. The (a) pressure increase the nominal case, and (b) the speciation for the nominal case with 1% residual air.

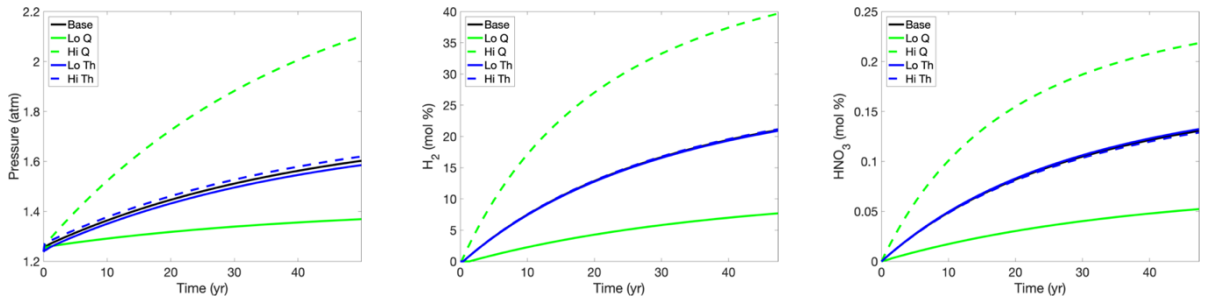

(a) (b) (c)

Fig. 9. The (a) pressure increase for all cases, the (b) hydrogen generated for all cases, and the (c) nitric acid generated for all cases (Q = decay heat, Th = corrosion layer thickness) for ATR fuel storage.

TABLE III. Results for a sealed canister with minimal bound water content for ATR fuel.

	Sealed Pure Helium			**Sealed + 1% air**			
Case / Variable Max	Pressure (atm)	H_2 (%)	O_2 (%)	Pressure (atm)	H_2 (%)	O_2 (%)	HNO_3 (ppm)
Base (18W, 10um thickness, 1% H2O(g))	1.36	7.3	3e-8	1.36	7.4	0.21	1562
Low decay heat (6W)	1.29	2.5	2e-8	1.29	2.2	0.21	565
High decay heat (42W)	1.51	16.2	7e-8	1.50	16.7	0.21	3070
Low Thickness (5 µm)	1.35	7.3	3e-8	1.34	7.3	0.21	1581
High Thickness (15 µm)	1.37	7.4	3e-8	1.37	7.4	0.21	1545

Undried Spent Fuel

If the fuel is not completely dried, pseudo boehmite may exists on the aluminum surface, allowing for thermal dehydration over time. This is reflected in the model with the maximum 2.5:1 H_2O:Al_2O_3 saturation ratio. When this is considered, there is a large spike in the pressure occurring over the first few months. This is a result of extrapolation of the reaction for the thermal dehydration of the boehmite over long periods of time. The result for the nominal case in pure helium for the pressure increase in shown in Fig. 10a, here the initial pressure spikes to 2.2 atm, with a slow increase to about 2.3 atm. The abundance of water vapor present makes these cases more suspectable to seasonal temperature changes in the canister gas content. The corresponding speciation for the nominal case shown in Fig. 10b. As with the previous cases, there is no other species present in large quantities other than water vapor, nitric acid and hydrogen for the case. In comparing this to results from the previous model with minimal bound water this is an uptick of about 0.9 atm. The results for the additional cases with variations in the initial residual water content, the decay heat of the fuel, and the corrosion layer thickness are shown in Fig. 11a for the pressure and Fig. 11b for the hydrogen content. These cases still show decay heat as the most dominant variable, with pressure variation of 0.7 atm, and hydrogen generation of 11 mole percent. With the potential for bound water to be released, the corrosion layer thickness does show a larger variation compared to the dried case at 0.4 atm, but only small changes in hydrogen.

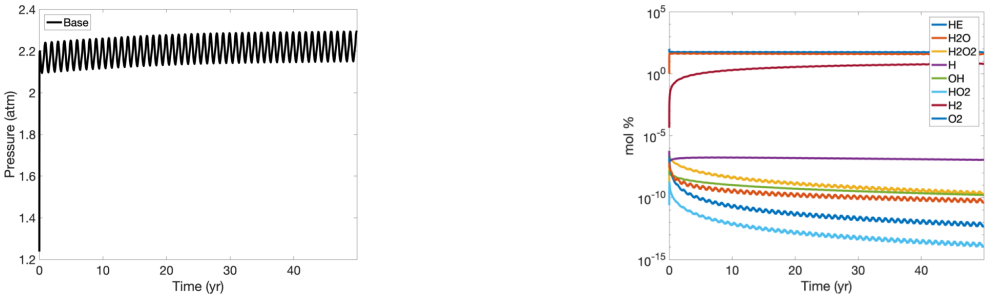

(a) (b)

Fig. 10. The (a) pressure increase and (b) the species generated for the nominal case in pure helium.

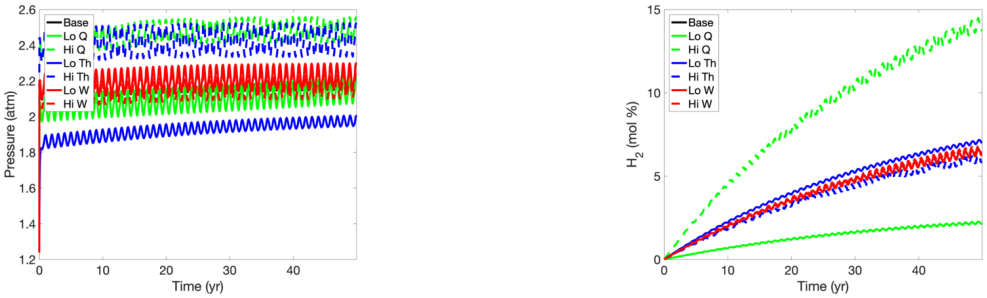

(a) (b)

Fig. 11. The (a) pressure increase and (b) the hydrogen generated for all cases in pure helium (Q = decay heat, Th = corrosion layer thickness, W = residual water).

The nominal case when considering a small amount of residual air shows only minor differences from the original case. The pressure for this nominal case is shown in Fig. 12a. This shows the large increase in pressure from thermal dehydration of pseudo-boehmite over the first couple of months followed by a slow evolution of the hydrogen generated from the aluminum oxyhydroxide layer. The speciation for this nominal case is shown in Fig. 12b. As with the dried case, only hydrogen and nitric acid are present in non-negligible amounts. The results for the variation in fuel decay heat, corrosion layer thickness and residual water are shown in Fig. 13a for the pressure increase. The pressure increase is nearly identical to the case with no residual air present. The results for the hydrogen generated are shown in Fig. 13b, as with pressure this is nearly identical to no residual air. The nitric acid concentration is shown in Fig. 13c with a variation after 50 years in the decay heat of 1600 ppm from low to high decay. Changes from corrosion layer thickness and residual water content are less then 100 ppm. The summary of the results is shown in TABLE IV.

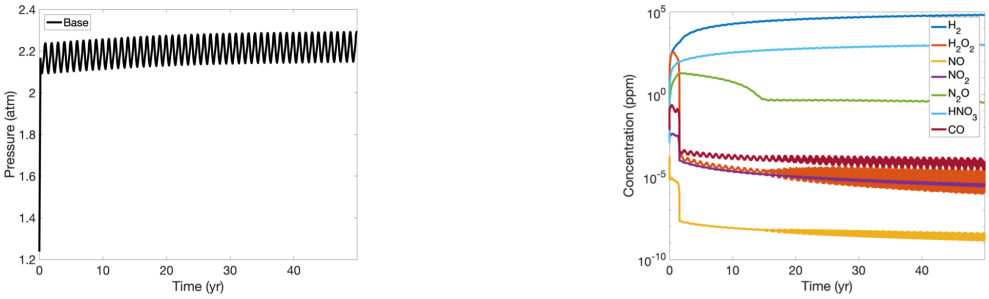

(a) (b)

Fig. 12. The (a) pressure increase, and (b) the species generated for the nominal case with 1% residual air.

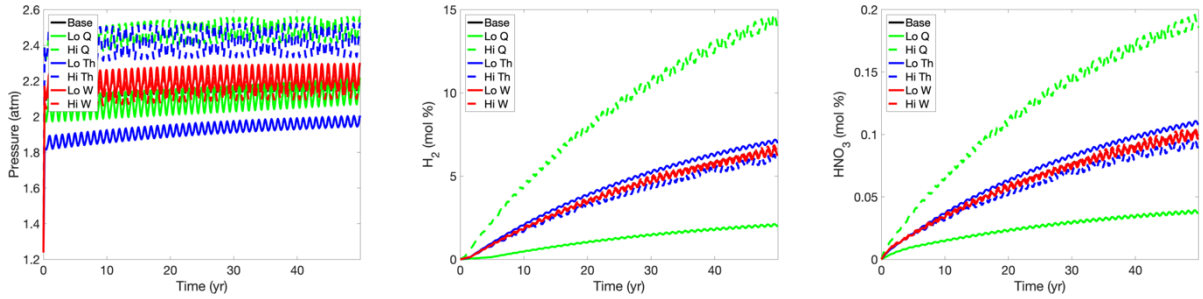

(a) (b) (c)

Fig. 13. The (a) pressure increase for all cases (b) the hydrogen generated and the (c) nitric acid generated for cases with 1% residual air (Q = decay heat, Th = corrosion layer thickness, W = residual water).

TABLE IV. Results for a sealed canister with minimal bound water content for ATR fuel with pseudo-boehmite assumption.

	Sealed Pure Helium			**Sealed + 1% air**			
Case / Variable Max	Pressure (atm)	H_2 (%)	O_2 (%)	Pressure (atm)	H_2 (%)	O_2 (%)	HNO_3 (ppm)
Base (18W, 10um thickness, 1% H2O(g))	2.29	6.7	2e-7	2.29	6.7	0.21	1028
Low decay heat (6W)	2.21	2.3	1e-7	2.21	2.1	0.21	394
High decay heat (42W)	2.56	14.5	6e-7	2.56	14.8	0.21	1957
Low H2O% (0.1%)	2.29	6.6	2e-7	2.3	6.7	0.21	1025
High H2O% (10%)	2.25	6.8	2e-7	2.25	6.9	0.21	1057
Low Thickness (5 µm)	2.0	7.2	5e-8	2	7.2	0.21	1108
High Thickness (15 µm)	2.52	6.3	5e-7	2.52	6.3	0.21	963

However, the concentrations reached do not approach the region where significant corrosion of the canister material would be expected to occur. At low concentrations of nitric acid, a range of expected stainless steel corrosion is about 0.01 to 0.034 mpy [35]. Significantly higher concentrations of nitric acid are needed for significant stainless-steel corrosion, at 4 molar HNO_3 this increases to 10 mpy.

CONCLUSION

A coupled CFD-chemical model was created for spent ATR fuel in backfilled DOE standard canisters intended for long term storage. The model shows that the initial decay heat of the packaged fuel is the primary variable of interest in dictating the results. The model itself shows nearly no dependence on the thickness of the corrosion layer, under fully dried fuel conditions. For undried conditions there is a slight dependency of the pressure due to potential additional water vapor release. The model was also tested with some small amount of residual air present, the effect of this is minor for the hydrogen concentration and pressure buildup, but does allow for the formation of other species, the highest of which is nitric acid.

Most scenarios modeled exhibit significant hydrogen above lower flammability limit, but no case shows this in combination any appreciable amount of oxygen, which is typically present in less than 1 ppb quantities. Of note, low decay heat cases for storage show a hydrogen value lower than the 4%

flammability limit; this decay heat roughly corresponds to 20 years after reactor discharge for spent ATR fuel. If a small amount of residual air is considered present, there is a possibility for 400-2000 ppm of nitric acid to form. Based on a brief literature survey, this concentration of nitric acid would only corrode the stainless steel at a rate between 0.01 to 0.034 mpy, negligible compared to the overall thickness of the canister. The nominal case shows a buildup of 1.36 total atmospheres with 7% total mole percent of hydrogen. The upper decay heat case shows an increase to 1.51 total atmospheres with 16% total mole percent hydrogen. For a worst case with undried fuel and high decay heat, this increases to 2.6 total atmospheres and 15% total mole percent hydrogen. These values of pressure are orders of magnitude less than the mechanically rated value of 34 atm (500 psi) for the DOE sealed standard canister.

Future research will include corrections for the G-value for hydrogen production at higher total doses, as initial testing done at Savanah River National Laboratory shows the G-value may decrease as a function of the total dose delivered. This will include a model of the mini canister for direct comparison of the hydrogen generation for validation of the chemical model. The timeframe of the current model will also be expanded, as most of the current results show that the hydrogen generation and pressure build up are still increasing at the end of the 50-year timeframe. This extension may be out to 100-200 years, or whenever the model shows an equilibrium or decline in the values. Lastly, the CFD model will be constructed for a planned 1/3rd size canister that will eventually be loaded with ATR fuel for an additional validation test.

ACKNOWLEDGEMENTS

This work was funded by the U.S. Department of Energy Environmental Management Office. This work was performed by Battelle Energy Alliance, LLC, under DOE Idaho Operations Contract DE AC07 05ID14517 and made use of the resources of the High Performance Computing Center at Idaho National Laboratory which is supported by the Office of Nuclear Energy of the U.S. DOE and the Nuclear Science User Facilities.

REFERENCES

1. SNFWG, “Aluminum Clad Spent Nuclear Fuel: Technical Considerations and Challenges for Extended (>50 years) Dry Storage.” Tech. Rep. Department of Energy, DOE/ID RPT 1575, (2017).

2. E.H. PARKER-QUAIFE and G.P. HORNE, Milestone 2.8: Preliminary Radiolytic Gas Generation Measurements from Helium-Backfilled Samples, Tech. Rep. Idaho National Laboratory, INL/EXT-21-61404, (2021).

3. M. NUSHIMURA, H. SHIBAZAKI, S. FUJII, and I. MAEKAWA, “Natural convection heat transfer in the horizontal dry storage system for the lwr spent fuel assemblies,” *Journal of nuclear science and technology*, 33, 11, 821–828, (1996).

4. S.Y. LEE, R.L. SINDELAR, and D.C. LOSEY, “Thermal modeling and performance analysis of interim dry storage and geologic disposal facilities for spent nuclear fuel,” *Nuclear technology*, 131, 1, 124–151, (2000).

5. X. HENG, G. ZUYING, and Z. ZHIWEI, “A numerical investigation of natural convection heat transfer in horizontal spent-fuel storage cask,” *Nuclear Engineering and Design*, 213, 1, 59–65, (2002).

6. R.A. BREWSTER, E. BAGLIETTO, E. VOLPENHEIN, and C.S. BAJWA, “Cfd analyses of the tn-24p pwr spent fuel storage cask.” In proceedings: ASME 2012 Pressure Vessels and Piping Conference. American Society of Mechanical Engineers, pp. 17–25, (2012).

7. D.G. LEE, J.H. PARK, Y.H. Lee, C.Y. BAEG, and H.J. KIM, "Natural convection heat transfer characteristics in a canister with horizontal installation of dual purpose cask for spent nuclear fuel," *Nuclear Engineering and Technology*, 45, 7, 969–978, (2013).

8. K.S. BANG, S.H. YU, S.H. LEE, J.C. Lee, and K.S. SEO, "Experimental investigation of heat removal performance of a concrete storage cask," *Annals of Nuclear Energy*, 85, 679–686, (2015).

9. Y.S. JEONG and I.C. BANG, "Hybrid heat pipe based passive cooling device for spent nuclear fuel dry storage cask," *Applied Thermal Engineering*, 96, 277–285, (2016).

10. B.L. SMITH, "Validation experiments for spent-fuel dry-cask in-basket convection." Tech. rep., Utah State Univ., Logan, UT (United States), (2016).

11. A.M. BULEARCA, I. CALINESCU, and V. LAVRIC, "Model Studies of NOx and SOx reactions in Flue gas treatment by electron beam," *UPB Sci Bull, Series B*, 72, 1, 101-112, (2010).

12. R. ATKINSON, D.L. BAULCH, R.A. Cox, J.N. CROWLEY, R.F. HAMPSON, R.G. HYNES, M.E. JENKIN, M.J. ROSSIE, and J. TROE, "Evaluated kinetic and photochemical data for atmospheric chemistry: volume I – gas phase reactions of X, HOx, NO2, and SOx species," *Atmospheric Chemistry and Physics*, 4, 6, 1461-1738, (2004).

13. O.P. ARKHIPOV, A.O. VERKHOVSKAYA, S.A. KABAKCHI, and A.N. ERMAKOV, "Development and verification of a mathematical model of the radiolysis of water vapor." *Atomic Energy*, 103, 5, 870, (2007).

14. A.W. ABBOUD and H. HUANG, "Full-scale Model of Dry Storage of Aluminum Clad Spent Nuclear Fuel, Rev. 1." Idaho National Laboratory, Tech. rep. INL/EXT-19-55185, (2019).

15. A.W. ABBOUD, "Modeling of ATR fuel in DOE Standard Canisters with Helium Backfilled Condition". Idaho National Laboratory, Tech. rep. INL/EXT-21-62306, (2021).

16. SIEMENS, User Guide: Star-ccm+ v14.06.011R8, (2019).

17. S.T. POLKINGHORNE and J.M. Lacy, "Thermophysical and Mechanical Properties of ATR Core Materials," Report No. PG-T-91-031, EG&G Idaho Inc., (1991).

18. F.P. INCROPERA, D.P. DEWITT, T.L. BERGMAN and A.S. LAVINE, *Fundamentals of Heat and Mass Transfer, Sixth Edition*, John Wiley and Sons, Hoboken, NJ, (2007).

19. D.B. ILLUM, "ATR Fuel Summary Report," Tech. Report INEL-96/300, 1996.

20. Lockheed Martin Idaho Technologies Co, Idaho National Engineering and Environmental Lab, Idaho Falls, ID, "Preliminary design specification for Department of Energy standardized spent nuclear fuel canisters Volume 1: Design specification" DOE/SNF/REP--011-Vol 1, (1998).

21. L.L. TAYLOR, "Packaging Strategies for Criticality Safety for Other DOE Fuels in a Repository," Tech. Rep., DOE/SNF/REP-90, (2004).

22. S.D. SNOW, "Design Considerations for the Standardized DOE SNF Canister Internals," Tech. Rep., DOE/SNF/DSN-19, (2008).

23. A. CHRISTENSEN, "EDF-2760, The Irradiated Fuel Storage Facility Maximum Heat Load And Resulting Maximum Temperatures When the Ventilation System Is Not Operating." Tech. rep., Idaho

National Laboratory, (2003).

24. A. CHRISTENSEN, "EDF-5579 Corrosion Potential of the Irradiated Fuel Storage Facility Environment." Tech. rep., Idaho National Laboratory, (2003).
25. A.K. WERTSCHING, T.J. HILL, N. MACKAY and S.M. BIRK, "Material Interactions on Canister Integrity During Storage and Transport." Tech. rep. Idaho National Laboratory, DOE/SNF/REP-104, (2007).
26. L. OLSON, C. VERST, A. D'ENTREMONT, R. FUENTES, and R. SINDELAR, "Characterization of Oxide Films on Aluminum Materials following Reactor Exposure and Wet Storage in the SRS L-Basin." Tech. Rep. Savannah River National Laboratory, SRNL-STI-2019-00058, (2019).
27. P. WINSTON, S. MIDDLEMAS, A. WINSTON, J. AGUIAR, X. LIU, and K. TOLMAN, "Aluminum Spent Fuel Performance in Dry Storage Task 4 Aluminum Oxide Sampling of ATR Dry Stored Fuel." Tech. rep. Idaho National Laboratory, INL/EXT-20-58404, (2020).
28. D. STEWART, 2012, ECAR-2906. "ATR Fuel Element In-Air Dose Rate Estimates Base on Heat Generation," Tech rep., Idaho National Laboratory, (2012).
29. R. WITTMAN, B. Hanson, "Radiolysis model analysis for a used fuel storage canister." In proceedings: IHLRWM April 2015, (2015).
30. D.G. GOODWIN, H.K. MOFFAT, and R.L. SPETH. *Cantera: An object-oriented software toolkit for chemical kinetics, thermodynamics, and transport processes*. http://www.cantera.org, Version 2.3.0. doi:10.5281/zenodo.170284, (2017).
31. M.L. WESTBROOK, R.L. SINDELAR, D.L. FISHER, "Radiolytic hydrogen generation from aluminum oxyhydroxide solids: theory and experiment," *J. Radioanal. Nucl. Chem.,* 303, pp 81-86, (2015).
32. T. LISTER and C. ORME, "Analysis of Vapor Phase Corrosion of Pretreated Aluminum Alloys." Tech. Rep. Idaho National Laboratory, INL/EXT-19-55558, (2019).
33. W. VEDDER and D.A. VERMILYEA. "Aluminum + Water Reaction." *Trans. Faraday Soc*., 65, pp.5 61-584, (1968).
34. B.A. HILTON, "Review of Oxidation Rates of DOE Spent Nuclear Fuel Part 1: Metallic Fuel." Tech. rep. Argonne National Laboratory, AN-00/24, (2000).
35. G.G. KOLMAN, D.K. FORD, D.K., D.P. BUTT, and T.O. NELSON, "Corrosion of 304 Stainless Steel exposed to nitric acid-chloride environments," *Corrosion Science*, 39, 12, 2067-2093, (1997).